DTU Library

Greenland meltwater storage in firn limited by near-surface ice formation

Machguth, Horst; MacFerrin, Mike; van As, Dirk; Box, Jason E.; Charalampidis, Charalampos; Colgan, William; Fausto, Robert S.; Meijer, Harro A. J.; Mosley-Thompson, Ellen; van de Wal, Roderik S. W.

Supplementary Figures | *Greenland meltwater storage in firn limited by near-surface ice formation*
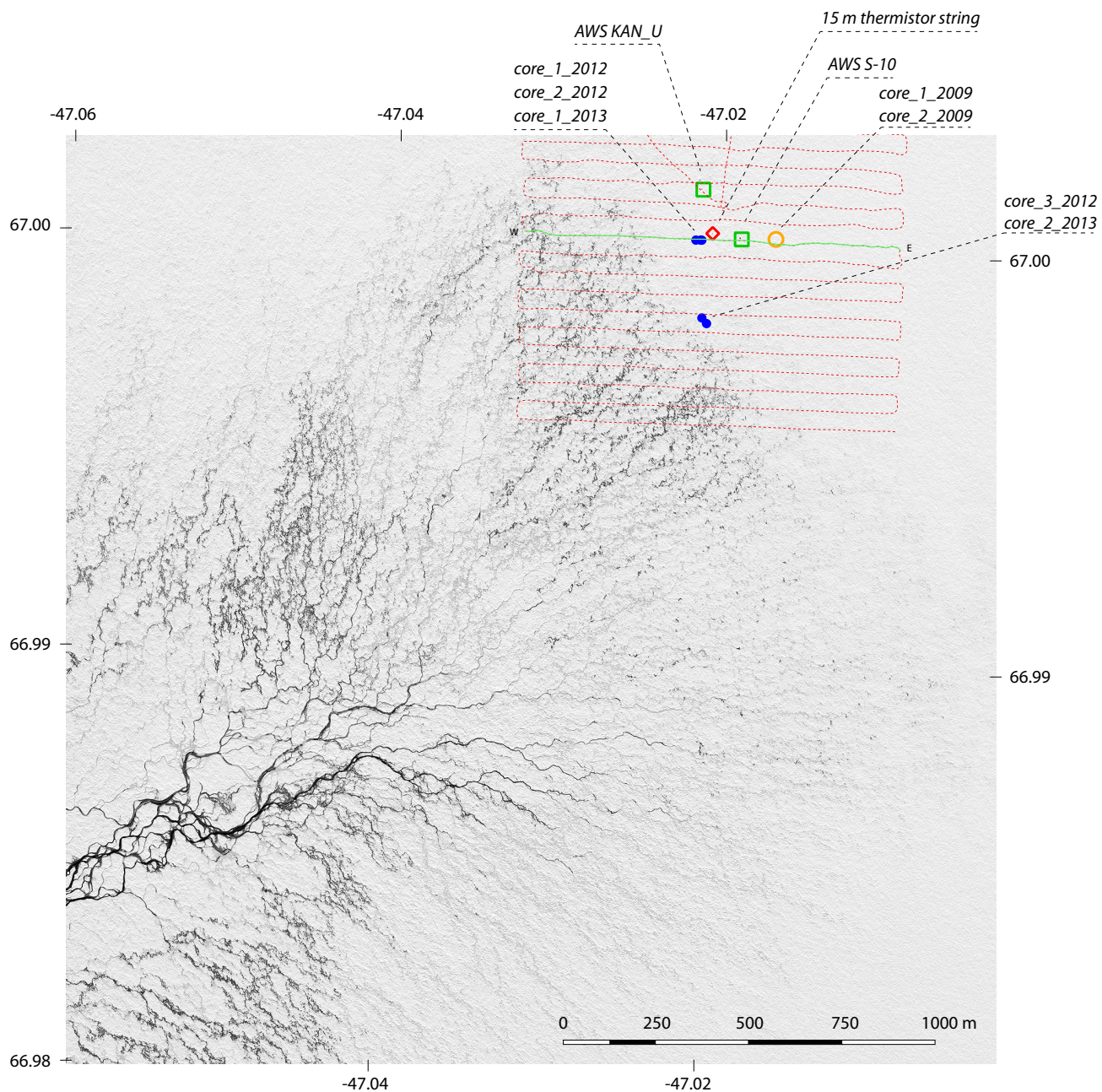
Supplementary Figure 1 | Melt features at the 1840 m site. Satellite image (WorldView1, panchromatic, 0.5 m spatial resolution) showing the area around the 1840 m site on August 12 2012. A snowfall event from August 6 and 7 has covered more narrow melt channels and some of the slush fields, but enhances contrast to the larger melt features. The dashed red line indicates the 1x1 km local radar grid from spring 2013 (about 1/4 of the grid lies north of the image frame), the green line highlights the radar profile shown in Supplementary Figure 3c. Locations of drill sites, automatic weather stations (AWS), radar grid and thermistor string locations are given for mid-2012, i.e. all 2013 coordinates are corrected for ice movement of ~50 m yr^{-1}.
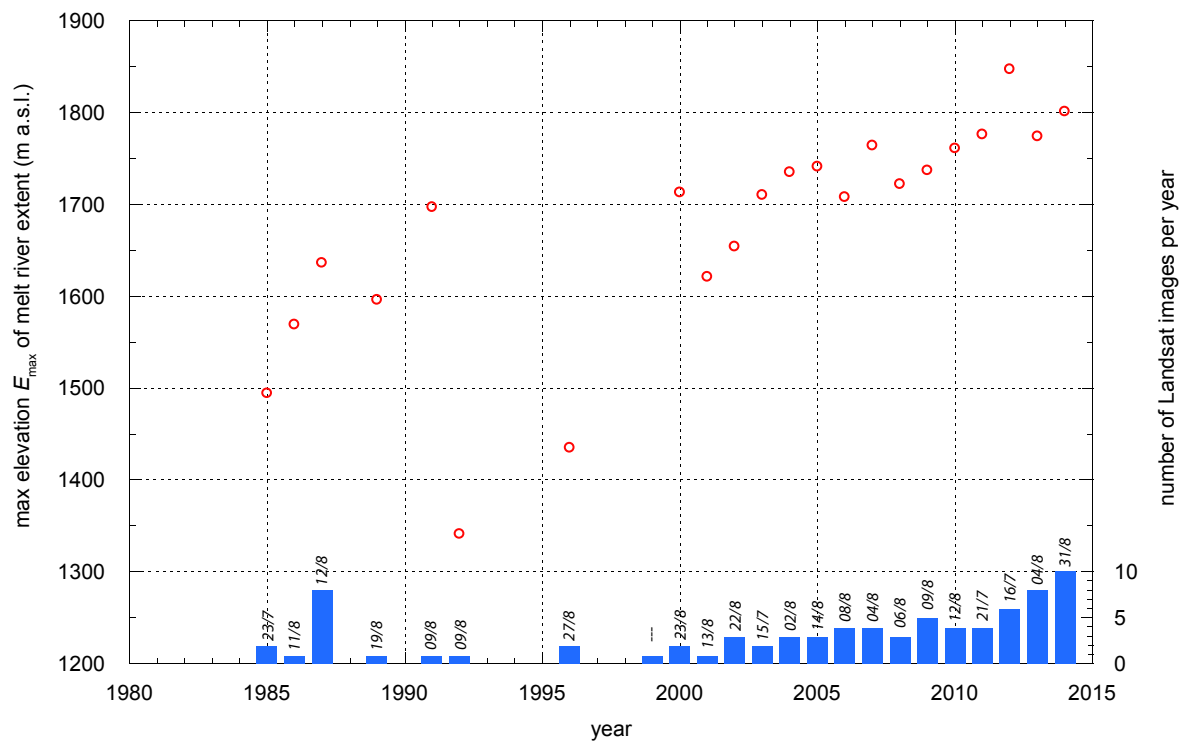
Supplementary Figure 2 | Maximum elevation E_{max} of supraglacial rivers (red circles) in the vicinity of the transect investigated in this study, as mapped from Landsat 4, 5, 7 and 8 imagery. Blue bars indicate the number of available Landsat images in the time frame July 15 to August 31 for every year. The date of the image showing the highest melt river extent is indicated on top of the bars.
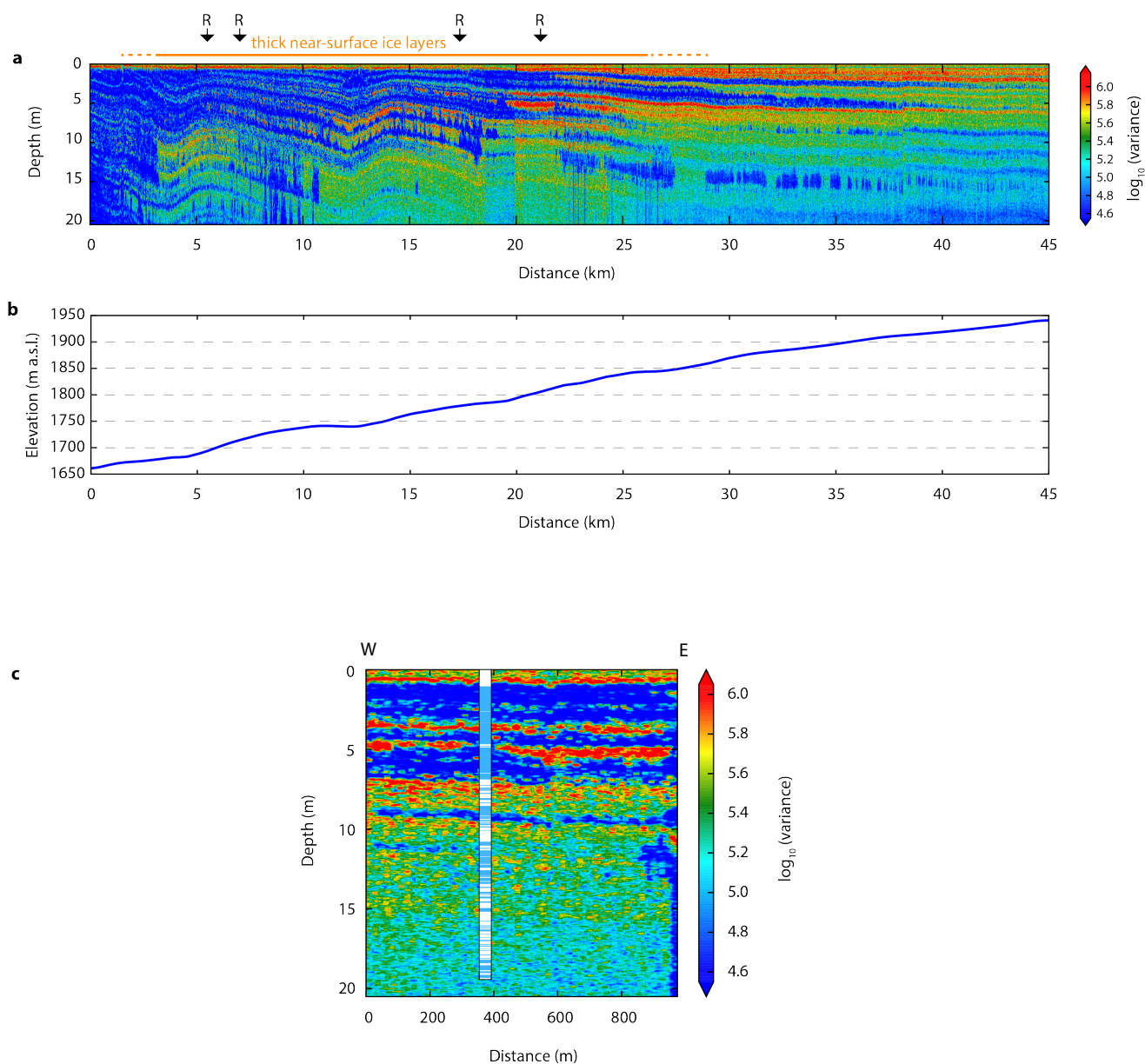
Supplementary Figure 3 | a, Lower 45 km (1660 to 1940 m a.s.l.) of the main radar profile along the 2013 core transect. Colours indicate density. At the high density limit, blue indicates ice and cyan to red indicates lower density firn. Vertical arrows with the letter "R" indicate the approximate location where the transect crosses the bed of larger meltwater rivers. "Larger" refers to rivers well recognizable on 15 m resolution panchromatic Landsat imagery from July 16 and August 17 2012. **b,** Hypsography of the ice sheet surface along the GPR transect (elevation is given in meters above the EGM2008 ellipsoid). **c,** Section of 2013 radar profile at the 1840 m site crossing the core location Core_1_2013. The stratigraphic profile of the core (ice lenses in blue) is overlaid onto the radar image for the purpose of direct comparison.
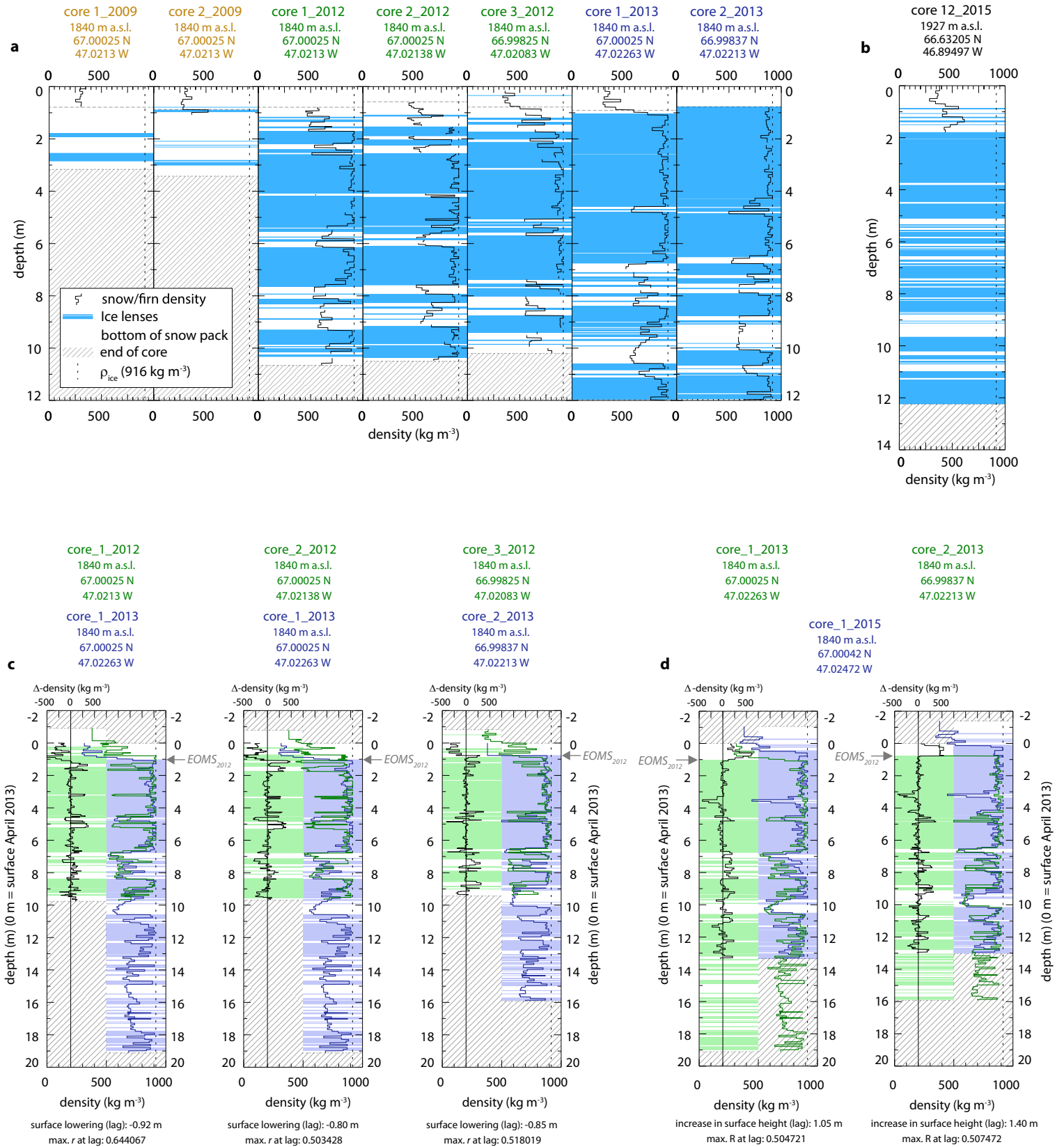
Supplementary Figure 4 | a, All firn cores drilled during the years 2009 to 2013 at the 1840 m site. Only the uppermost 12 m are shown to optimize visual comparison (the complete core_1_2013 and core_2_2013 are shown in Fig. 2). **b**, Stratigraphy of core_12_2015, drilled in May 2015. **c**, Alignment of cores drilled at the 1840 m site in spring 2012 (green) and spring 2013 (blue). **d**, As pannel (c), but aligning cores from spring 2013 (green) and a core from spring 2015 (blue). $EOMS_{2012}$ indicates the end-of-melt-season 2012 surface. Surface lowering indicated at the bottom of each plot in pannels (c) and (d) refers to the change in surface height from end of April 2012 to end of April 2013 (in pannel (d): end of April 2013 to end of April 2015) and corresponds to the upward shift of the 2012 (2015) cores with reference to the 0 m depth level. Surface lowering (increase in surface height) refers to the time period from spring 2012 to spring 2013 (spring 2013 to spring 2015). The maximum linear regression coefficient of the density profiles in each pair is denoted with r.
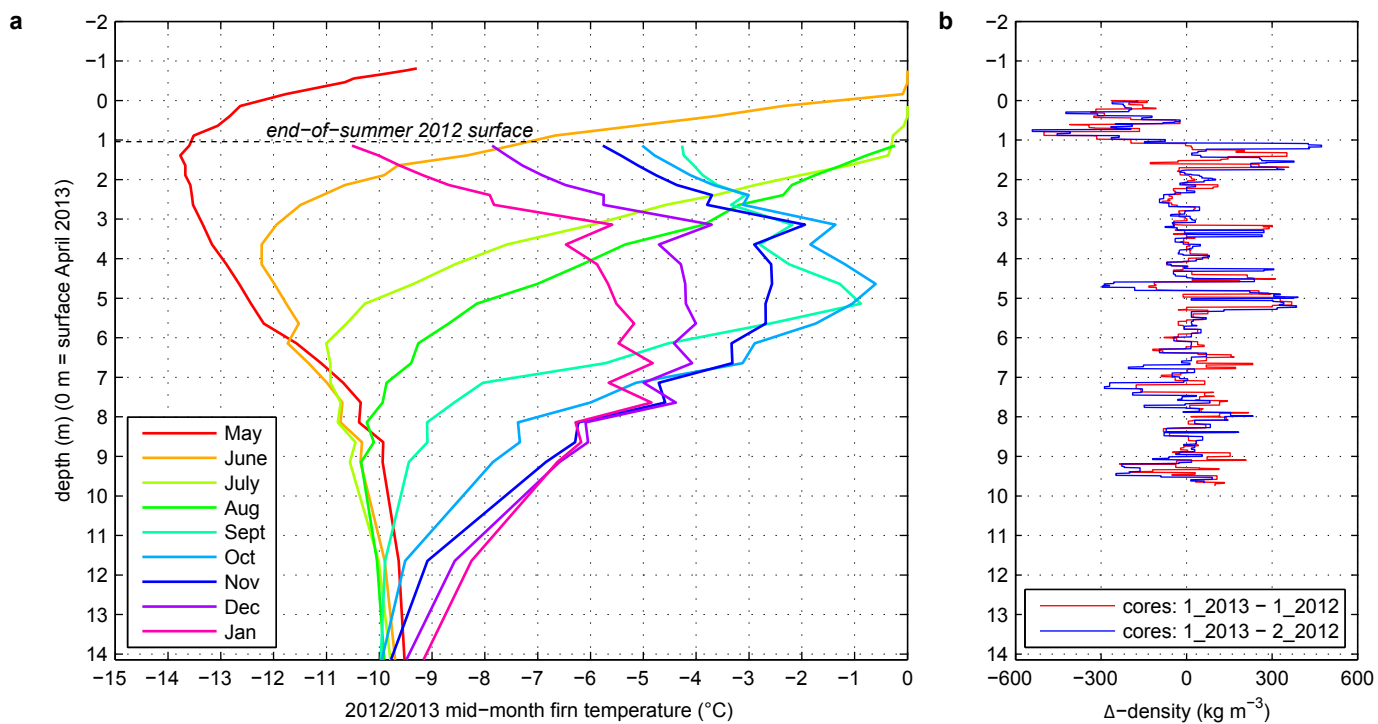
Supplementary Figure 5 | a, Monthly average firn temperature depth profiles measured by the 15 m thermistor string at the 1840 m site, illustrating seasonal fluctuations and the pronounced September warming centred at 5 m depth. **b,** Associated changes in density for the two pairs of cores located in close proximity (~15 m) to the thermistor string.
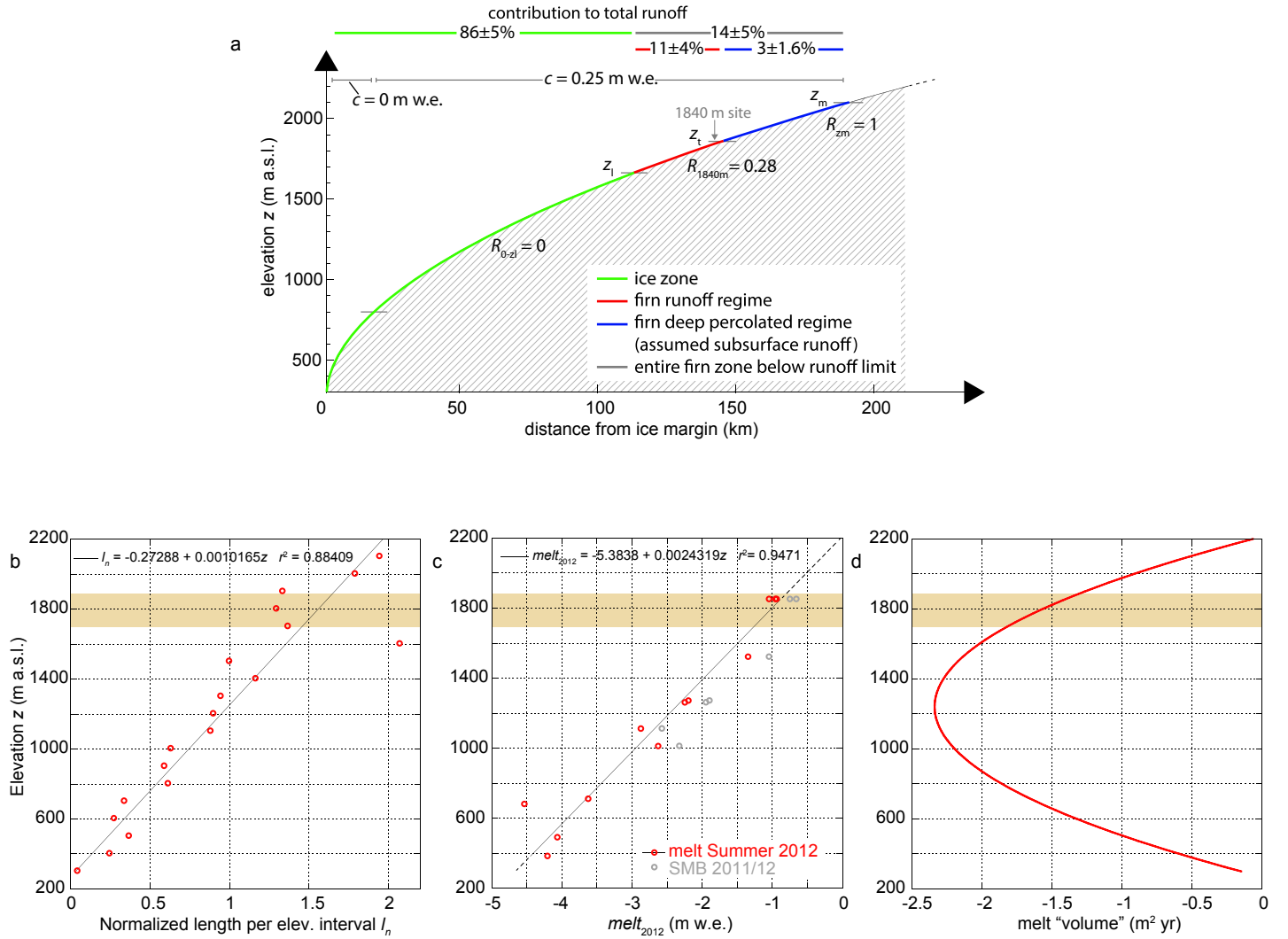
Supplementary Figure 6 | a, Concept of the runoff calculation along the K-Transect elevation profile. The lower limit of the zone of thick near-surface ice layers is denoted z_l, the upper limit z_t and the runoff limit z_m. The fraction of total melt that is retained is denoted with R_{0-zl}, R_{1840m} and R_{zm}, accumulation is c. **b,** Normalized transect-length of 100 m elevation intervals along the K-Transect from 300 m a.s.l. to 2200 m a.s.l. and linear fit. **c,** Elevation profile of surface melt for the time period from spring 2012 to the end of August 2012. Grey circles indicate annual mass balance from August 2011 to August 2012 prior to melt adjustment. Dotted lines indicate where the linear fit is extrapolated beyond the elevation range covered by measurements. **d,** Melt "volume" per elevation interval resulting from multiplication of the linear regressions of $melt_{2012}$ and l_n. The orange shading in the plots b, c and d indicates the vertical extent of the zone of thick near-surface ice layers as inferred from the radar profiles.

6
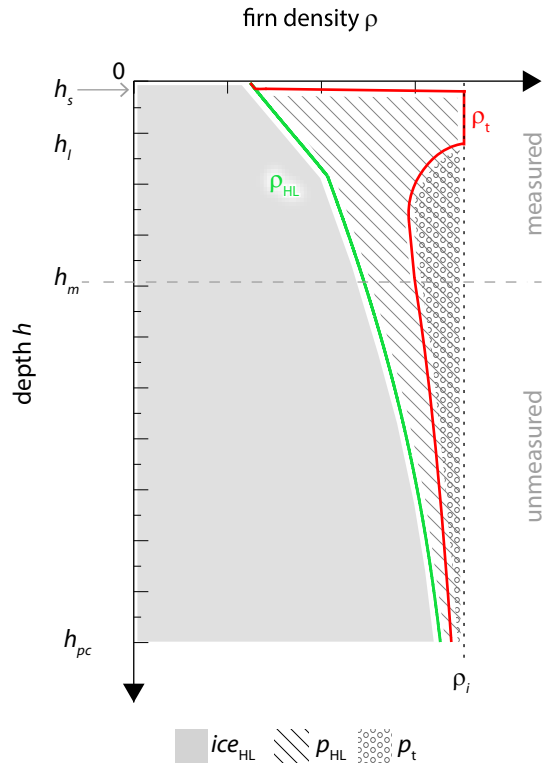
Supplementary Figure 7 | Schematic illustration of the different components of the firn. Ice_{HL} refers to the volume occupied by ice under conditions with only dry snow densification [8], p_{HL} is the pore space under dry firn conditions and p_t is the observed transient (relict) pore space. The bottom depth of the snow pack is h_s, h_l is the bottom depth of the thick near-surface ice layers, h_m is the bottom depth of the firn-core measurements. Pore close-off depth is denoted with h_{pc}. To emphasize $h_s \neq 0$, an arrow is added.

Supplementary Tables | *Greenland meltwater storage in firn limited by near-surface ice formation*

Supplementary Table 1 | Parameters and output of the MC simulation of runoff partitioning

a

parameter	value	uncertainty	unit
c	0.25	0.1	m w.e.
z_0	300	-	m a.s.l.
z_l	1680	30	m a.s.l.
z_t	1870	30	m a.s.l.
z_m	2100	50	m a.s.l.
R_{1840m}	0.25	0.25	-
a	0.0027288	0.0002060	-
b	0.0010165	8.93e-005	-

b

elevation interval	runoff contribution (%)	standard deviation (%)
300 – 1680 m a.s.l.	85.8	4.9
1680 – 2100 m a.s.l.	14.2	4.9
1680 – 1870 m a.s.l.	11.2	4.1
1870 – 2100 m a.s.l.	3.0	1.6

a, Parameters in the MC simulation of runoff partitioning, chosen values and uncertainties (one standard deviation). Accumulation is c, z_0 is the lowermost elevation of the profile, z_l is the lower boundary elevation of the thick near-surface ice layers zone, z_t is the upper boundary elevation of the thick near-surface ice layers, z_m is the runoff limit, the fraction of total melt that is retained at the 1840 m site is denoted with R_{1840m}. The two variables a and b are the slopes of the linear regressions of transect length versus elevation and 2012 summer melt versus elevation, respectively. **b**, Contribution to runoff from different elevation intervals along the K-Transect calculated with the MC simulation. The computation encompasses 5000 runs, the runoff contributions and related standard deviations are calculated based on the 3457 valid runs (69% of all runs).

Supplementary Table 2 | Parameters and output of the MC simulation of relict pore space at the 1840 m site

a

parameter	value	uncertainty	unit
h_s	0.90/0.78	-	m
h_l	7.5	0.5	m
h_m	19.12/15.94	-	m
h_{pc}	(54.4)	(7.6)	m
T_a	-15	2	°C
P_a	0.35	0.1	m w.e.
ρ_i	873	25	kg m^{-3}
f_r	(0.43/0.40)	0.2	-

b

core	depth range	
	measured	entire firn column
Core_1_2013	0.27±0.05	0.34±0.10
Core_2_2013	0.24±0.05	0.31±0.10

a, Parameters in the MC simulation of relict pore space volume at the 1840 m site, chosen values and uncertainties (1 standard deviation). Where two values are given the first relates to Core_1_2013 and the second to Core_2_2013. Values in brackets are not prescribed but calculated from the MC model. The bottom depth of the snow pack is h_s, h_l is the bottom depth of the thick icelayers, h_m is the bottom depth of the measurements and pore close off-depth is denoted with h_{pc}. Mean annual air temperature and accumulation at the 1840 m site are T_a and P_a, respectively. The mean density of ice layers is ρ_i and f_r is the fraction of relic pore space in the depth range h_l to h_m **b**, Relic pore space expressed as fractions of dry firn pore space, calculated in an MC simulation for the two cores Core_1_2013 and Core_2_2013 and over measured depth range (h_s to h_m) as well as the entire firn column (h_s to h_{pc})

Supplementary Text | *Greenland meltwater storage in firn limited by near-surface ice formation*

Supplementary Methods

GPR Processing

Raw GPR data collected from the Malå 800 MHz shielded GPR Rx/Tx antenna provided average spacing of 1.42 m between traces, which was later resampled using a nearest-neighbour approach to even 1.5 m spacing. Locations of GPR traces recorded between GPS locations were linearly interpolated. Dewow and linear gain filters were applied to all traces to remove low-frequency artefacts and enhance the signal at depth, respectively. A moving window spanning three traces horizontally (4.5 m) by thirteen samples vertically (1.3 ns, the span of one complete 800 MHz radar waveform) measured the variance of the signal in the immediate neighbourhood surrounding each sample pixel. Thick lenses, having a homogeneous physical structure compared to the surrounding firn, result in a lower variance than samples within more porous and heterogeneous firn. Speed of electromagnetic waves in firn was chosen at 202.6 m μs^{-1}, which maximized the negative correlation between core density and the variance and is consistent with other studies[30], and led to an average radar survey depth of the top 20.5 m of firn. GPR data were processed in their original 16-bit signed integer format as the gain/bias conversion from digital number to signal power would not enhance the signal further. A maximum local variance of 56,200 ($10^{4.75}$, 16-bit local-neighbourhood signal variance) was chosen to identify ice layers, maximizing the agreement between ice lenses identified in the GPR traces and stratigraphy measured manually at each core location. Using this method, ice lenses ≥0.23 m thickness and spanning at least 4.5 m horizontal distance can theoretically be distinguished in the radar signal, while thinner lenses are lost in processing. Given the practical consideration that thin ice lenses tend to refreeze in a highly spatially heterogeneous manner (unlike thicker layers that span larger spatial distances)[9], we found that we could realistically identify lenses ≥0.8 m thick spanning ≥20 horizontal meters in the firn.

Fraction of relict pore space

The concept of quantifying pore space fractions at the 1840 m site is visualized in Supplementary Fig. 7. The density profile ρ_{HL} for dry snow densification according to[8] defines the maximum potential firn pore space and is here used as our 100% reference pore volume. The transient firn density ρ_t (Supplementary Fig. 7) reflects the present-day profile which is, in contrast to the reference pore space, strongly influenced by refreezing of meltwater. Furthermore we measured ρ_i = 873±25 kg m^{-3} as the mean density of all 0.1 m core sections in Core_1_2013 to Core_7_2013 that consist to 100% of visually identified ice (n = 245; cores at or above the elevation of core_8_2013 are excluded because there are very few 0.1 m sections of pure ice).

The density profile below h_m is unmeasured. However, measurements of ice layer frequency in two nearby 1989 cores (Site J, 2030 m a.s.l., drilled to ~200 and ~100 m depth[29], cf. Fig. 1) indicates a rather constant firn regime over most of the 20th century. Thus it is assumed that ice layer frequency in the unmeasured firn at the 1840 meter site is of similar characteristics as the measured firn between h_l and h_m.

Each of the two firn density profiles involves a characteristic amount of reference pore space p_{HL} and transient pore space (p_t). We calculate ρ_{HL} according to[8] using mean annual air temperature T_a = -15 °C and accumulation $P_a = 0.35$ m w.e. yr^{-1} according to the meteorological observations at the 1840 m site[15] corrected for recent warming of 1°C. The reference pore space available for melt storage is given by $p_{HL} = \int_{h_s}^{h_{pc}} \rho_i - \rho_{HL} \, dh$, the transient pore space by $p_t = \int_{h_s}^{h_{pc}} \rho_i - \rho_t \, dh$, where h_{pc} and h_s are the pore-close-off depth and the bottom of the snow pack, respectively. The snow cover is excluded from the calculations as we focus on firn, whose pore space is, in contrast to the snow cover, not completely renewed annually. The observed transient pore space is considered difficult to access for meltwater storage, is thus termed "relict pore space", and is expressed as a fraction of reference pore space $f_r = p_t/p_{HL}$. The above calculations require knowing $\rho_t(h)$ below the bottom depth h_m of the firn core. Based on the aforementioned data from Site J[29], we here we assume that f_r in-between the bottom depth h_l of the thick ice layers and h_m, is representative for the unmeasured depth range h_m to h_{pc} ($h_{pc} = 54$ m according to ρ_{HL} (z) for a pore close-off density of 830 kg m^{-3}).

The MC uncertainty in calculated relict pore fraction is performed analogously as for the calculation of firn area contribution to overall runoff (see Methods). Parameters used in the calculation are listed in Supplementary Table 2 and parameter uncertainties are given where applicable.

A total of 5000 runs are performed and in each run the parameters ρ_i and the calculated fraction of relict pore space in the depth range h_l to h_m (f_r) are checked for validity. The density of ice lenses has to be in the density range from pore close off (830 kg m^{-3}) to pure ice (917 kg m^{-3}). The parameter f_r cannot fall below 0 or exceed 1. The calculation is performed for both cores drilled at the 1840 m site in 2013, yielding almost identical results (Supplementary Table 2).

Supplementary Discussion

Calculation of summer 2012 mass balance and retention at 1840 m a.s.l.
Direct comparison of core stratigraphies is an uncommon approach to quantify surface melt and retention. Concerns with the accuracy of this approach might be raised as firn stratigraphy can vary substantially over short horizontal distances[9] on the order of 1 to 10 m. Our investigation of 6 cores drilled in close vicinity at the Core_7 site (2150 m a.s.l., cf. Fig. 1) indicates considerable variability of stratigraphic detail over distances from 10 to 140 m (not shown here). The approach applied at 1840 m a.s.l. is nevertheless considered valid for the following reasons.
   (i)   Study[9] highlights an increased lateral continuity in firn profiles at lower elevations where some ice lenses considered to be multi-annual features exceed 0.5 m in thickness. Most ice lenses at 1840 m a.s.l. exceed this threshold.
   (ii)   In spring 2012 and 2013 ground radar grids of 1 by 1 km at 100 m spacing and centred on the 1840 m site were recorded (Supplementary Figure 1). The data show little variations in firn stratigraphy; for example, the firn lens present at 5 m depth in spring 2012 can be traced continuously. The same is the case for the ~1 m ice layer at 8 m depth (Supplementary Figure 3).
   (iii)   When comparing the 2012 and 2013 cores, the disappearance of the firn layer at 5 m depth is the most obvious change in stratigraphy. The sudden autumn 2012 warming of the firn to 0 °C (Supplementary Fig. 5) is centred on the same depth and indicates that the firn layer acted as a pathway for melt water trapped in-between ice layers. While

refreezing, the latent-heat release warmed the firn and the porous interstitial firn horizon was filled.

(iv) The calculated values of surface melt (-0.98, -0.93 and -0.83 m w.e.) and retention (0.27, 0.29 and 0.14 m w.e.) are similar. Further, the surface melt rates agree well with melt (-1.00 and -0.91 m w.e.) derived from mass balance measured at stakes and the two weather stations operated at the site. The melt has been calculated by subtracting measured snow cover by end of April 2012 (0.26 m w.e.) from the measured annual mass balance (referring to the time period August 2011 to August 2012).

While the calculation of surface melt is considered robust, the derivation of subsurface retention is more ambiguous. Each of the three profiles of $\Delta\rho$ also includes depth sections where $\Delta\rho$ is negative. This is most likely caused by lateral discontinuities of thinner ice lenses[9]. However, positive values in $\Delta\rho$ might have the same origin and thus cannot be unambiguously assigned to pore space filling by refreezing melt water. Hence, the cause of density changes in the subsurface can only be determined with certainty where additional information is available, such as the thermistor string data. For these reasons the retention is calculated based on $\Delta\rho$ shallower than 5.2 m. All differences in density at greater depths are assigned to lateral discontinuity of ice lenses. In fact, the difference in density, averaged over the three pairs of cores and the depth range 5.2 m to bottom of the 2012 cores is small (6 kg m^{-3}), but the standard deviation of density changes at 0.1 m intervals is large (105 kg m^{-3})[$\Delta\rho$ and related standard deviation for the individual pairs of cores: 22±84 kg m^{-3} for *Core_1_2013 - Core_1_2012*; -25±102 kg m^{-3} for *Core_1_2013- Core_2_2012*; 21±120 kg m^{-3} for *Core_2_2013 - Core_3_2012*]. These small overall differences together with large standard deviations support the assumption of an unchanged firn pack at depth where differences among the cores result primarily from lateral discontinuities of ice lenses. Furthermore, a slight increase in density at depth is expected due to natural firn compaction.

Contribution of 2012 firn-area runoff to total melt water discharge
We calculate the contribution to runoff from three distinct elevation bands and assess uncertainties of the partitioning. The regional scale assessment's primary goal is to evaluate the impact of firn processes on melt water availability. Hence the term *runoff* refers to liquid water that is not retained and enters a highly efficient[7] supraglacial discharge network.

The calculation is performed along an elevation transect where melt is well constrained from observational data. No direct measurements of melt exist elsewhere in the vicinity of the transect but the snowline on the available satellite imagery (Fig. 1) suggests that major longitudinal variations in melt were absent. The hypsometry of the chosen transect is a good representative of the ice sheet elevation profile in the region (Fig. 1). Aiming at a regional scale estimate, melt and hypsometry are both generalized by use of linear regressions. A linear fit represents the characteristics of the melt profile well ($r^2 = 0.947$). For hypsometry a linear fit ($r^2 = 0.884$) is chosen as well because of straightforwardness and more complex regressions result in a negligible increase in goodness of fit (r^2 equals 0.888 and 0.885 for a 2nd degree polynomial and a power law, respectively).

The calculation along a transect furthermore eases comprehensive computation of uncertainties utilizing a Monte Carlo (MC) approach to determine overall uncertainty based on input parameter uncertainties. Uncertainties in the elevations z_l and z_t are based on the analysis of the radar image which allows confident determination of the elevation of z_l. The image shows no clear upper margin of the thick near-surface ice layers, but above 1840 m a.s.l. ice lenses rapidly decrease in thickness.

Further, it is known that at 1840 m a.s.l. the near-surface ice layers exhibit a strong impact on runoff. For these reasons z_t is set to 1870 m a.s.l., an elevation rather close to the 1840 m site. Both elevations z_l and z_t are assigned an uncertainty of 30 m. These uncertainties are considered rather large, given that the vertical extent of the thick near-surface layers is roughly 200 m.

In the ablation area and the elevation zone of the thick near-surface ice layers parameters are relatively well constrained from melt observations. The latter, however, are missing from the firn area above the zone of thick near-surface ice layers. It is reasonable to assume a further decline in melt and an increase in the retention potential of the firn above the thick near-surface layer zone. The runoff limit z_m is positioned at 2100 m a.s.l. where melt according to the linear regression amounts to ~0.25 m w.e. It is assumed that this amount of melt can be fully retained because the less porous firn at 1840 m a.s.l. retained the same amount of melt water. However, uncertainties are large as can be illustrated on the example of melt: According to the linear fit, melt is zero at ~2250 m a.s.l. while observations indicate that melt occurred even at the ice sheet summit (3220 m a.s.l.)[5] at least for one day in 2012. Apparently the melt curve is nonlinear for elevations above the range of measurements. Nevertheless, the linear regression is deemed valid for the purpose of runoff partitioning because core data provide no evidence that any of the small amount of melt generated in the shallow-percolation firn regime exited the ice sheet. To avoid a strong underestimation of melt for the zone above the uppermost melt measurements at 1840 m a.s.l., we reject in the MC simulation all runs where the linear regression of melt results in a zero melt altitude of less than 2100 m a.s.l. The relatively limited amount of melt above the thick near-surface ice layer zone is also the main reason for the small contribution of high elevations to total runoff (Supplementary Table 1); the relatively large associated uncertainty reflects the challenges in defining parameter values.

The fraction of melt water retained in the firn R_z is approximated using two linear functions – (1) from $R_z = 0$ at $z = z_l$ to $R_z = 0.25$ at $z = 1840$ m a.s.l., and (2) $R_z = 0.25$ at $z = 1840$ m a.s.l. to $R_z = 1$ at $z = z_m$. Over the course of the entire 2012 melt season it appears justified to assume negligible retention at z_l [3]. The linear functions are chosen because (i) the radar and the firn cores show a more or less continuous decrease in ice layer thickness with elevation (Fig. 2 and Supplementary Fig. 3), and (ii) retention fraction is only measured at the 1840 m site. To account for this strong dependency on a single measurement we assigned a large uncertainty of 0.25 to R_{1840} in the MC simulation. Furthermore also z_l and z_m are subject to variation in the MC simulation which, in combination with the large uncertainty range of R_{1840}, guarantees that strongly varying linear functions are applied.

Maximum elevation extent of supraglacial melt rivers, 1985 to 2014
Melt rivers are mapped on Landsat imagery as they are the most obvious expressions of surface runoff. Landsat is a logical choice for this task because of being the only freely available data covering a long time period and offering sufficiently high spatial resolution to recognize individual melt rivers. Since we are interested in the elevation extent of surface runoff, our goal is also fundamentally different from analysis of passive microwave remote sensing data which provide coarse resolution maps of surface melt extent[5] but do not provide any information about runoff.

Here we define a river head as the elevation of the uppermost image pixel that is considered being part of the linear structure on the image, representing the river. An exact quantification of the actual size of the mapped rivers cannot be given as the image resolution (15 to 30 m) is too coarse to allow measuring width of the features. On the example of the river originating at the 1840 m site, its

appearance on panchromatic 15 m resolution Landsat 7 (August 17 2012) and 0.5 m resolution WorldView1 (August 12 2012) can be directly compared. It is found that rivers of 5 to 7 m width are already well recognizable on the Landsat image due to the pronounced contrast between dark water and surrounding lighter ice.

The approach of mapping melt river elevation extent on Landsat imagery involves uncertainties related to (i) the limited number of Landsat scenes available per melt season, and (ii) to subjective decision making in picking the five highest river heads within the buffer. Although the number of available scenes is small in most summers, at least one scene for every summer could be found that is of sufficient quality for accurate mapping. Comparing scenes for years where more than one suitable image is available within the time frame July 15 to August 31 shows that vertical melt river extent does not depend strongly on the date, i.e. the rivers do not appear or disappear suddenly. For instance, in summer 2012 the difference of melt river extent mapped on scenes from July 16 and August 17 is only 13 m. Decision making in picking melt river heads is helped by the fact that the major melt rivers always appear on the same locations. Once one has familiarized with the pattern of the rivers, it is easy to map the same rivers every year and to thereby optimize interannual comparability of the mapping. The geographical stability of the major rivers helps in finding and recognizing them even after snow fall events. For these reasons we consider the Landsat analysis to show reliably that the melt river extent of the summer 2012 stands out compared to all other years.

An important limitation of the approach is the inability of quantifying the intensity of surface runoff. This becomes most apparent when comparing imagery from summer 2012 to earlier or later summers: While the maximum elevation of melt river extent in 2012 exceeds some of the other years only by 50 to 70 m, the distribution of melt features on the surface is qualitatively different. In 2012 the entire surface up to an elevation close to the maximum extent of melt rivers (1850 m a.s.l.) is completely snow free and dominated by countless smaller and larger melt channels (Fig. 1 and Supplementary Fig. 1). In 2014, for instance, major rivers reach similar elevations (~1800 m a.s.l.), but down to an elevation of approximately 1700 m a.s.l. these rivers are surrounded by areas still snow covered. The latter is not an effect of a snow fall event, as it can be observed on all available scenes.

Fraction of relic pore space
We calculated the amount of pore space rendered relic and expressed it as a fraction of dry firn pore space. Thereby the latter is our estimate of the total pore space available for melt water storage. Hence, calculating a relict pore space fraction of 32±10% also means assuming that 68±10% of the pore space has been used for melt water storage. The latter assumption implies that pore space filling through refreezing is the sole process that has modified a dry firn profile into the observed density profile. While it appears justified to assume that dry firn compaction and refreezing are the two dominant processes that have shaped the observed firn profiles, both processes always coexisted at the site (most likely even during the Little Ice Age[29]) and have influenced each other. The probably most important feedback process is that latent heat release associated with refreezing in the firn column has accelerated dry firn compaction, which makes it likely that the total amount of pore volume available to store melt water is lower than the dry firn pore space calculated according to [8]. For this reason the calculated dry firn pore space is a conservative upper bound estimate of the pore space available for melt water storage. Whenever this reference pore space volume would be reduced (i.e. shifting the line denoted with ρ_{HL} to the right in Supplementary Fig. 7), then the *fraction* of relic pore space f_r increases. While this does not affect the absolute amount

of relict pore space, it means that the calculated fraction of total pore space should be considered a lower bound estimate.

The major challenge in calculating the relict pore space volume is the limited length of the firn cores at the 1840 m site when compared to an estimated pore-close-off depth at 53 m. Here we assume that f_r observed below the thick near-surface ice layers is representative for the unmeasured depth range. As explained in the methods section, the assumption is founded in two nearby cores where an effectively constant fraction of melt features in the firn column over the 20th century was observed[29]. Nevertheless, a large uncertainty of 0.2 by fraction is assigned to the calculated value of f_r (0.41 and 0.39 for the two cores Core_1_2013 and Core_2_2013, respectively). An MC simulation where f_r, is treated as the sole uncertain parameter yields an overall uncertainty (±0.08 or ±0.09 for Core_1_2013 and Core_2_2013, respectively) similar to the value based on all and interacting parameter uncertainties (Supplementary Table 2). Rather wide uncertainty ranges have been chosen for the other parameters as well, but the extrapolation to the unmeasured depth range is the major source of uncertainty in the calculation of relic pore space.

Additional references

[30] Kovacs, A., Gow, A. and Morey, R. The in-situ dielectric constant of polar firn revisited. *Cold. Reg. Sci. Technol.* **23,** 245-256 (1995).